

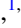



Spin-wave nonreciprocity at the spin-flop transition region in synthetic antiferromagnetsO. Gladii ¹, R. Salikhov ¹, O. Hellwig ^{1,2}, H. Schultheiss^{1,3}, J. Lindner¹ and R. A. Gallardo ⁴¹*Helmholtz-Zentrum Dresden-Rossendorf, Institute of Ion Beam Physics and Materials Research, Bautzner Landstrasse 400, D-01328, Germany*²*Institute of Physics, Chemnitz University of Technology, Reichenhainer Strasse 70, D-09107 Chemnitz, Germany*³*Technische Universität Dresden, 01069 Dresden, Germany*⁴*Departamento de Física, Universidad Técnica Federico Santa María, Avenida España 1680, Valparaíso, Chile*

(Received 8 September 2022; revised 20 February 2023; accepted 28 February 2023; published 20 March 2023)

We investigate the frequency nonreciprocity in CoFeB/Ru/CoFeB synthetic antiferromagnets near the spin-flop transition region, where the magnetic moments in the two ferromagnetic layers are noncollinear. Using conventional Brillouin light scattering, we perform systematic measurements of the frequency nonreciprocity as a function of an external magnetic field. At near zero magnetic field, where the antiparallel alignment of the magnetic moments in the two layers is established, we observe a significant frequency nonreciprocity of up to a few GHz, which vanishes when the relative magnetization orientation switches into the parallel configuration at a large magnetic field. For the intermediate values of the magnetic field, where the system transitions from the antiparallel to the parallel orientation, a nonmonotonous dependence of the frequency nonreciprocity is found, with a maximum frequency shift around the spin-flop critical point. This nontrivial dependence of the nonreciprocity versus field is attributed to the nonmonotonous dependence of the dynamic dipolar interaction, which is the main factor that causes asymmetry in the dispersion relation. Furthermore, we found that the sign of the frequency shift changes even without switching the polarity of the bias field. These results show that one can precisely control the nonreciprocal propagation of spin waves via field-driven magnetization reorientation.

DOI: [10.1103/PhysRevB.107.104419](https://doi.org/10.1103/PhysRevB.107.104419)**I. INTRODUCTION**

Spin-wave nonreciprocity, where the wave characteristics depend strongly on the inversion of the propagation direction, attracts a particular interest due to its high technological relevance. Inspired by this effect, concepts of magnon logic devices [1], diodelike spin-wave emitters [2–4], and unidirectional caustic beam generators [5] have been proposed. Furthermore, by employing magnetoelastic coupling, the spin-wave nonreciprocity can be converted to acoustic nonreciprocity, resulting in acoustic isolators and circulators [6–9]. The spin-wave nonreciprocity requires magnetic materials or artificial systems with a broken space-reversal symmetry. For example, chiral magnets can host nonreciprocal spin waves due to Dzyaloshinskii-Moriya interaction (DMI) [10,11]. On the other hand, the symmetry breaking at the surface/interface between a ferromagnetic material and material with a strong spin-orbit coupling gives rise to interfacial DMI [12–14]. Although the amplitude of interfacial DMI-induced nonreciprocity is typically one order of magnitude larger than that induced by bulk DMI, its contribution rapidly decays within a few nanometers away from the surface.

The classical dipole-dipole interaction can also induce spin-wave nonreciprocity in certain types of nanostructures, such as magnetization-graded films [15], curvilinear magnetic shells [16–21], arrays of nanopillars [22], coupled ferromagnetic bilayers [23–33], and magnonic crystals [34,35]. In the case of antiparallel coupled bilayers [synthetic antiferromagnets (SAFs)], a highly nonreciprocal spin-wave propagation has been observed, where the nonreciprocity is induced by

an interlayer dipole-dipole interaction resulting in asymmetric mode profiles [27,31,32]. In contrast to interfacial DMI-induced frequency shift, which is present only in ultrathin magnetic films, the dipole-induced nonreciprocity increases with the film thickness and thus is more notable in thick films. The advantage of using thick ferromagnetic layers is the possibility to achieve large spin-wave group velocities occurring as the film thickness increases and, respectively, large spin-wave propagation lengths, which considerably facilitate the study and control of spin waves in magnetic systems. Moreover, the use of a magnetic SAF system provides an additional degree of freedom in the manipulation of spin waves, namely switching its reciprocal character from strongly nonreciprocal to completely reciprocal depending on the relative magnetization orientation of the magnetic layers [27].

While the origin of the spin-wave nonreciprocity in synthetic antiferromagnets, which is the dynamic dipolar interaction between the adjacent ferromagnets, was elucidated in Ref. [27], the present work addresses a simple but fundamental question about the impact of dynamic dipolar interaction on the spin-wave nonreciprocity in a noncollinear magnetization state. To answer this question, we properly designed our samples, utilizing the control of magnetic parameters, and we investigated the field-dependent nonreciprocal propagation of spin waves in in-plane SAF trilayer systems using Brillouin light scattering. We demonstrate that the frequency nonreciprocity exhibits a nonmonotonous dependence in the transition region from antiparallel to parallel alignment of the magnetic moments with a maximum nonreciprocity around the spin-flop critical point. Our experimental

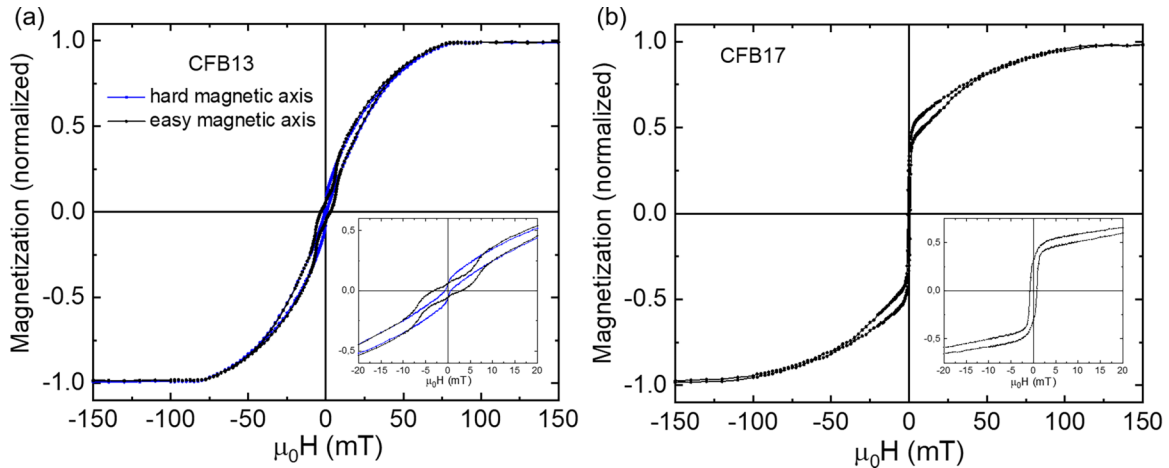


FIG. 1. Magnetic hysteresis loops measured with a magnetic field applied parallel to the film surface for (a) CFB13 and (b) CFB17 samples. The insets show an enlarged view of the corresponding hysteresis loops at small magnetic fields.

finding is supported by numerical calculations, which additionally demonstrate that the origin of such nonmonotonous dependence stems from the nonmonotonous dependence of the dynamic dipolar interaction as we vary the relative orientation of the static magnetizations. Thereby, the present work provides a handle to accurately control the nonreciprocal propagation of spin waves via the field-driven magnetization reorientation within the SAF. Our concept can be potentially extended to any noncollinear magnetic texture in multilayers (for example, domain walls), which can be used as a spin-wave medium [36,37].

II. SAMPLES AND EXPERIMENTAL TECHNIQUE

To study the spin-wave nonreciprocity near the spin-flop transition region, as prototype systems, we use SAFs, which possess two $\text{Co}_{40}\text{Fe}_{40}\text{B}_{20}$ (in at. %) ferromagnetic layers with easy-plane anisotropy. The antiferromagnetic (AF) coupling between the two ferromagnetic layers is stabilized by Ruderman-Kittel-Kasuya-Yoshida (RKKY) interaction using a 0.58-nm-thin Ru spacer. The Ru thickness is optimized as a compromise between the AF coupling strength and reduced biquadratic contribution to the interface coupling [38]. The biquadratic coupling term decreases when increasing the Ru layer thickness [39,40]. We consider two types of SAFs: (i) with symmetric stack, where the thickness of the two CoFeB layers is identical $t_1 = t_2 = 13$ nm; and (ii) asymmetric stack, where $t_1 = 17$ nm and $t_2 = 9$ nm. The full stack of our samples reads Ta(5 nm)/CoFeB(13 nm)/Ru(0.58 nm)/CoFeB(13 nm)/Ta(2 nm) and Ta(5 nm)/CoFeB(17 nm)/Ru(0.58 nm)/CoFeB(9 nm)/Ta(2 nm), which we refer to as CFB13 and CFB17, respectively. The 2-nm-thin Ta layer is used as a cap layer to protect the magnetic stack from oxidation. The 5-nm-thin Ta seed layer serves for better adhesion. In addition, we find in the symmetric stack that the biquadratic coupling term is reduced at 5 nm Ta seed, while it is still quite strong for a 3 nm Ta seed.

All samples are fabricated at room temperature by dc-magnetron sputter deposition at 0.4 Pa (3 mTorr) Ar atmosphere in a high-vacuum system (ATC 2200, from AJA

International Inc.). We use Si substrates with a 100-nm-thick thermally oxidized (SiO_2) layer. During the deposition, the substrate is rotated at about 60 rpm. All target guns are inclined at an angle of 30° with respect to the normal of the substrate. The thickness of all layers is controlled by deposition time. Prior to the sample fabrication, the sputter rate of each material was calibrated using x-ray reflectivity. Magnetic properties of the samples are characterized at ambient conditions using a commercial Microsense EZ7 vibrating sample magnetometer (VSM), equipped with a 1.8 T electromagnet.

The spin-wave propagation in magnetic SAF trilayers has been studied using wave-vector resolved BLS in backscattering geometry. A schematic illustration of the sample is sketched in Fig. 2(d). The sample is illuminated by a laser beam of wavelength $\lambda = 532$ nm, where the angle of the incident light θ is fixed to 45° , which allows exciting spin waves with a wave vector of $k = (4\pi/\lambda)\sin(\theta) = 16.7 \mu\text{m}^{-1}$. The magnetic field is applied in the film plane and perpendicular to the wave propagation. The BLS spectra are recorded for different values of the applied magnetic field (± 160 mT) to establish a field-dependent variation of the resonance frequency. The frequency nonreciprocity is quantified by comparing the BLS spectrum at positive and negative magnetic fields.

III. RESULTS AND DISCUSSIONS

A. Magnetic properties

In-plane magnetic hysteresis loops for the studied systems are presented in Fig. 1. Both loops display an ‘‘S-shape’’ behavior due to a remaining contribution of the biquadratic coupling term [39,40]. The saturation magnetization of both samples is measured to be $M_s = 1100$ kA/m. The nonzero remanence in the CFB13 symmetric sample, seen in the inset of Fig. 1(a), indicates that the two CoFeB magnetic moments are not fully antiparallel at zero field. Considering a simple macrospin model, we calculate the angle of 175° between the two directions of the magnetic moments. According to Refs. [39,41,42], we estimated the bilinear (J_1) and biquadratic (J_2) coupling terms from the hysteresis loops to be $J_1 = -0.41 \pm 0.04$ mJ/m² and $J_2 = -0.07 \pm 0.02$ mJ/m²

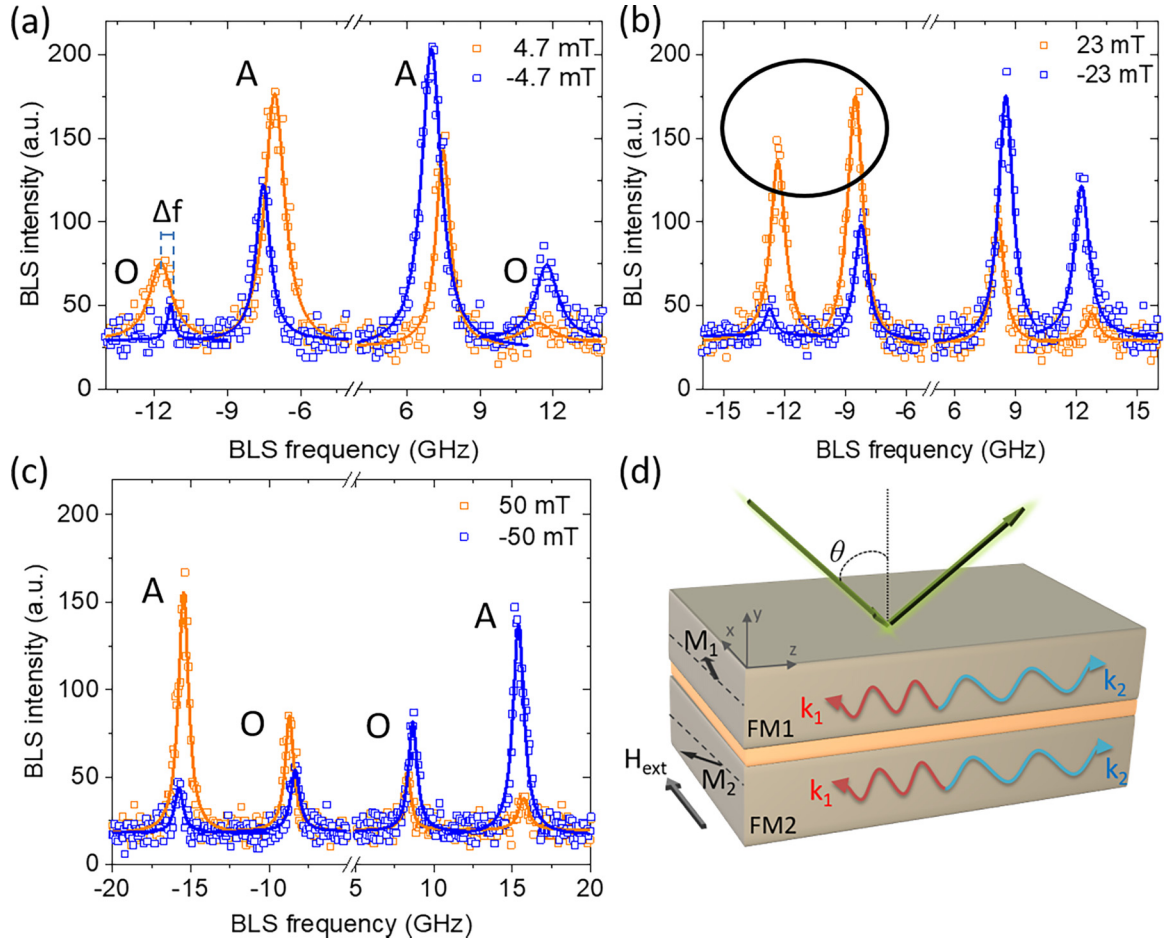


FIG. 2. (a)–(c) BLS spectrum measured in CoFeB(17 nm)/Ru(0.58 nm)/CoFeB(9 nm) film at different values of applied magnetic field. The variation of the resonance frequency of optic (O) and acoustic (A) modes and the change of their amplitudes as a function of the magnetic field are depicted. The frequency nonreciprocity (Δf) of a given mode is measured as the difference between the peak positions at positive and negative fields, as exemplarily shown for the optic mode in (a). The circle in (b) highlights the convergence of acoustic and optic mode amplitudes. (d) Schematic of the studied sample, illustrating the nonreciprocal spin-wave propagation in the SAF. The orientation of magnetizations M_1 and M_2 illustrates the states in the spin-flop region.

for the CFB13 symmetric sample, and $J_1 = -0.6 \pm 0.06$ mJ/m² and $J_2 = -0.08 \pm 0.03$ mJ/m² for the CFB17 asymmetric sample. These experimentally extracted values were also used as input parameters for the dynamic calculations, which we present and discuss below. At this point, we conclude that due to the significant biquadratic contribution, the alignment of magnetizations at an external magnetic field is not fully antiparallel and, therefore, the spin-flop region extends from almost zero field to the field at saturation, thus allowing us to systematically study the spin-wave nonreciprocity for different magnetic moment configurations of the two ferromagnetic (FM) layers (from almost antiparallel to almost parallel) by varying the external field. Finally, we find a small growth-induced in-plane uniaxial anisotropy, which is evident by comparing the hysteresis loops measured along a hard (blue curve) and easy (black curve) magnetization axis as shown in the inset of Fig. 1(a). This anisotropy results from the oblique deposition with the easy magnetization axis being perpendicular to the atomic flux direction [43,44]. Accordingly, the easy magnetization axis can be predefined by experimental geometry. Note that the field-dependent BLS

measurements are performed with the external field applied parallel to the easy magnetization axis.

B. Spin-wave frequencies

Figures 2(a)–2(c) present the BLS spectra of the CFB17 sample for different magnetic field directions and strengths. Each spectrum composes four peaks, where the two peaks with negative (positive) frequencies correspond to Stokes (anti-Stokes) modes. The two Stokes or two anti-Stokes peaks are attributed to different modes in the coupled trilayer structure: optic mode, which involves the out-of-phase precession of dynamic magnetizations in the two ferromagnetic films, and acoustic mode, which represents their in-phase precession. Note that the categorization of the modes (optic and acoustic) is based on the theoretical model described in Appendix A, where the magnetization orbits are calculated. At a magnetic field of 4.7 mT [Fig. 2(a)], the low-frequency mode with a higher signal amplitude corresponds to the acoustic mode, and the high-frequency mode with a lower signal amplitude corresponds to the optic mode. By increasing the

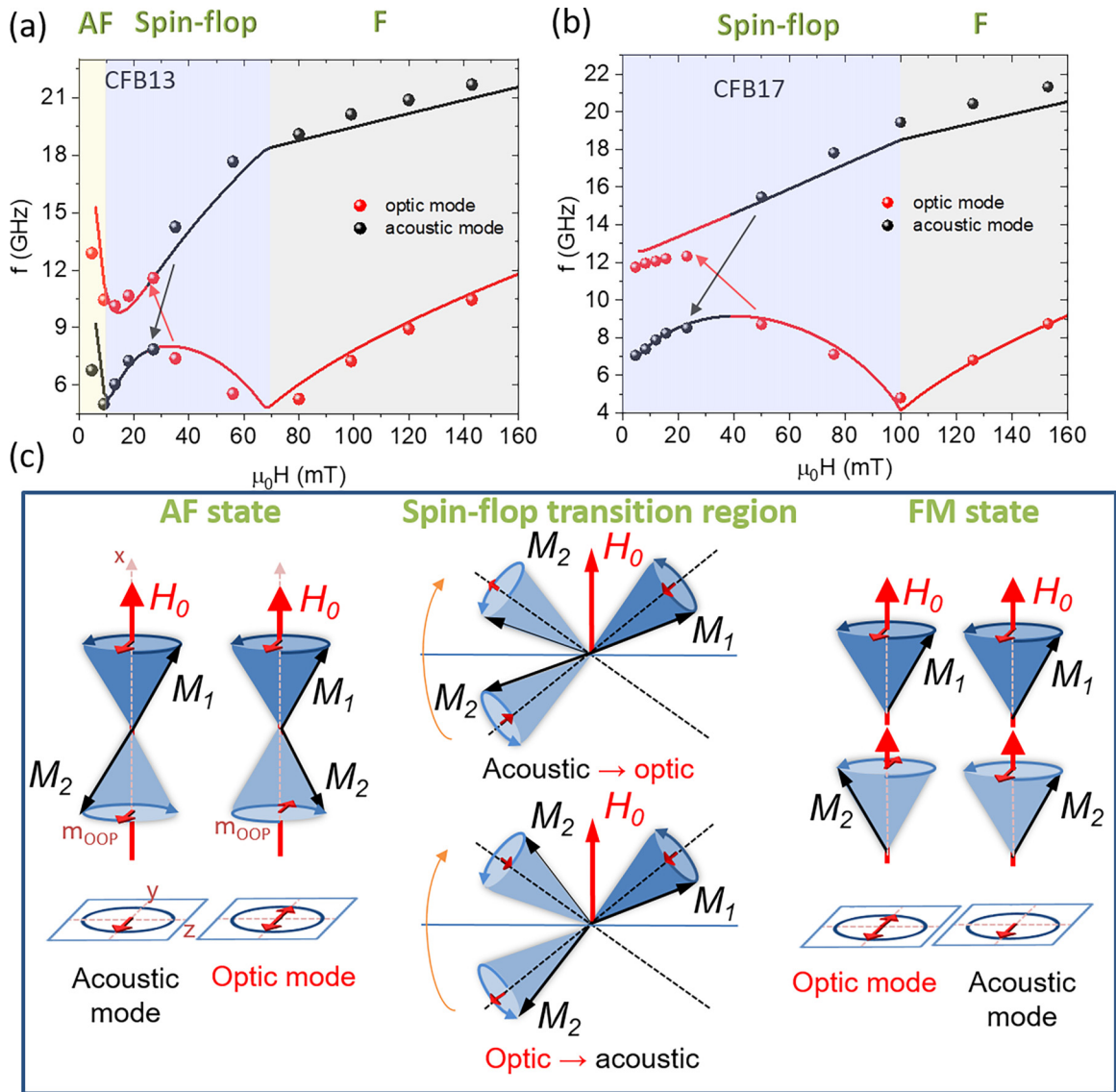


FIG. 3. Stokes frequency dependence on applied positive magnetic field measured in CFB13 (a) and CFB17 (b) films. Experimental data are shown by symbols, while the solid lines show the numerical calculations. The arrows indicate the frequency jump of the optic and acoustic modes from the high-frequency branch to the low one and vice versa. Differently colored areas indicate the three magnetic states: antiferromagnetic (AF), spin-flop, and ferromagnetic (FM). (c) Schematic representation of optic and acoustic modes in the three different magnetization states and their transition from one state to another. For details, see the main text.

magnitude of the bias field, both the peak position and the peak amplitude change. At 23 mT, the optic and acoustic modes move towards each other, and their amplitudes become comparable [Fig. 2(b)]. Then, at a higher field [Fig. 2(c)], the modes move away from each other, and the low-frequency mode becomes the one with lower amplitude (so it becomes an optic mode), while the high-frequency mode becomes the mode with higher amplitude (it becomes an acoustic mode).

The variation of the peak positions, i.e., the variation of the BLS frequencies as a function of the applied magnetic field, is plotted in Figs. 3(a) and 3(b) for both samples, where the experimental data are represented by symbols, and the lines correspond to the calculated modes (see Appendix A for details). At a sufficiently high magnetic field, the FM state is established, where the magnetization in both layers is aligned towards the direction of the applied magnetic field.

The schematic representation of optic and acoustic modes in the FM state is illustrated on the right side of panel (c). In this state, the acoustic mode is characterized by the in-phase precession of both in-plane (IP) and out-of-plane (OOP) components of dynamic magnetization, while the optic mode represents their out-of-phase precession [note that for simplicity and for further comparison with magnetization precession in the AF state, the OOP components only are sketched in Fig. 3(c)]. In the FM region, the frequencies of both modes decrease by lowering the magnitude of the applied magnetic field, which is related to a reduction in Zeeman energy. At some point (70 and 100 mT for CFB13 and CFB17, respectively), the frequencies of the optic modes reach their minimum and then start to increase again, while the frequencies of the acoustic modes gradually decrease by decreasing the magnetic field.

Then, an interchange of the precession phases occurs, and the optic mode “jumps” to the high-frequency branch, while the acoustic mode “jumps” to the low-frequency one [shown by arrows in Figs. 3(a) and 3(b)]. The observed field-dependent variation of the resonance frequencies is related to the fact that the magnetic moments in the two FM layers are no longer collinear since the amplitude of the applied magnetic field is not sufficient anymore to counterbalance the interlayer exchange interaction and, hence, the angle between the magnetic moments of both layers becomes field-dependent.

The rotation of magnetic moments from ferro- to antiferromagnetic alignment occurs in the so-called spin-flop transition region, where the maximum of the low-frequency mode corresponds to an orthogonal orientation of the magnetic moments [45,46]. The interchange of the mode phases at this critical point can be understood from the illustration presented in the middle panel of Fig. 3(c): an in-phase precession of dynamic magnetization transforms to an out-of-phase precession as soon as the projection of M_2 on the field axis (H_0) changes its sign. Therefore, the acoustic mode becomes the optic mode and vice versa. In the spin-flop regime, magnetization M_2 presents opposite in-plane local orientations. This transition occurs because M_2 has almost zero precessional angle in the intermediate transient state. With a further increase of H_0 , the precessional angle increases again together with a 180° phase shift.

By further lowering the magnetic field, the magnetic moments in the two layers tend to align antiferromagnetically. Contrary to the FM state, in the AF state, the acoustic and optic modes are defined exclusively by the OOP component's relation [as shown on the left of panel (c)]: their in-phase precession describes the acoustic mode and their out-of-phase precession describes the optic mode [6]. Such a definition allows us to explain the energy of both modes in a quasi-AF state, which is reached in the CFB13 trilayer for an external field below 10 mT [Fig. 3(a)]. However, due to the strong elliptical precession of magnetization, the deflection angle of the precession is very different within the film plane as compared to the out-of-plane case, where such an out-of-plane magnetization component corresponds to the minor axis of the elliptical precession. Therefore, the acoustic mode is considered as a low-frequency mode, since the out-of-plane magnetization projections are parallel while the in-plane components are antiparallel. On the other hand, the out-of-phase oscillation of the out-of-plane magnetization components (m_{OPP}) implies an in-phase oscillation of the in-plane components [see the left panel in Fig. 3(c)], indicating a higher dynamic coupling energy of the system, and thus the mode with higher frequency is classified as “optical.”

The measured frequency dependencies on the applied magnetic field were fitted using the theory developed in Ref. [27], where the dynamic dipolar interaction between the FM layers is considered. A good agreement between the theoretical and experimental data was found, where the fitted parameters of the symmetric CFB13 sample are as follows: $M_s = 1070$ kA/m, anisotropies in both layers $\mu_0 H_{u1} = 0$ and $\mu_0 H_{u2} = 5.5$ mT, interlayer exchange $J = -0.35$ mJ/m², and biquadratic term $J_2 = -0.07$ mJ/m². This last term was necessary to reproduce well the experimental results.

On the other side, the magnetic parameters used for the asymmetric CFB17 sample were $M_{s1} = 1100$ kA/m and $M_{s2} = 1070$ kA/m. Here, subscript 1 (2) corresponds to the CoFeB layer of 17 nm (9 nm) thickness. This small difference in the saturation magnetizations was considered to explain the finite frequency shift observed at high fields, which will be shown below. In addition, $\mu_0 H_{u1} = 1$ mT and $\mu_0 H_{u2} = 5$ mT; $J_1 = -0.22$ mJ/m², and $J_2 = -0.22$ mJ/m². In addition, a perpendicular anisotropy field $\mu_0 H_s = 150$ mT was used. It is worth mentioning that for sample CFB17, the biquadratic term is much larger than for CFB13, as well as comparing to the value extracted from the magnetometry measurements. We suspect that the disagreement is related to a twisted magnetization state in the 17-nm-thick layer. Indeed, this thickness is comparable to the characteristic exchange length of the CoFeB, which can lead to magnetization twisting (the magnetization at the two interfaces within the layer thickness is not strictly collinear in the spin-flop transition region). At the same time, the interface roughness (which contributes to the dipolar interaction between the ferromagnetic layers) may also play a crucial role in the magnetization dynamics and lead to a difference between magnetometry and BLS data. Therefore, instead of introducing further parameters (exchange stiffness and its in-depth variation, asymmetric pinning parameters at the Ta and Ru interfaces, interlayer roughness, etc.), we simulated the data by varying the existing parameters in our macrospin model. However, these parameters may not reflect the exactly correct experimental values anymore. In addition, a perpendicular anisotropy field was introduced in order to improve the fitting. The calculations also confirm the mode interchange, as follows from the phase difference calculated at the resonance frequency of each mode.

C. Nonreciprocal spin-wave propagation

We will now analyze the evolution of the frequency nonreciprocity for different magnetic states. We define the frequency nonreciprocity Δf as the frequency shift between the corresponding resonance modes recorded at positive and negative fields of the same amplitude, so $\Delta f = f_{O/A}(+H) - f_{O/A}(-H)$. In Fig. 4, the dependence of the frequency nonreciprocity on the external magnetic field is shown for both samples. As one can see, in both cases, the frequency nonreciprocity varies nonmonotonously as we increase the amplitude of the external magnetic field. For the CFB13 sample, a large nonreciprocity of about 1.5 GHz is measured at a small magnetic field, where a quasi-AF alignment is present, while a zero frequency nonreciprocity is detected for ferromagnetic alignment. This observation is consistent with previously reported data, where the same behavior of spin-wave propagation was found in exchange-coupled magnetic bilayers [27]. The large Δf in the AF alignment was attributed to a different *dynamic dipolar interaction* for positive and negative k , which occurs as a result of different relative orientations of the dynamic stray field and the dynamic magnetization in the SAF with opposite static magnetization alignments. In fact, this dipole-dipole interaction also plays a significant role in the nonmonotonous frequency nonreciprocity, which will be discussed below.

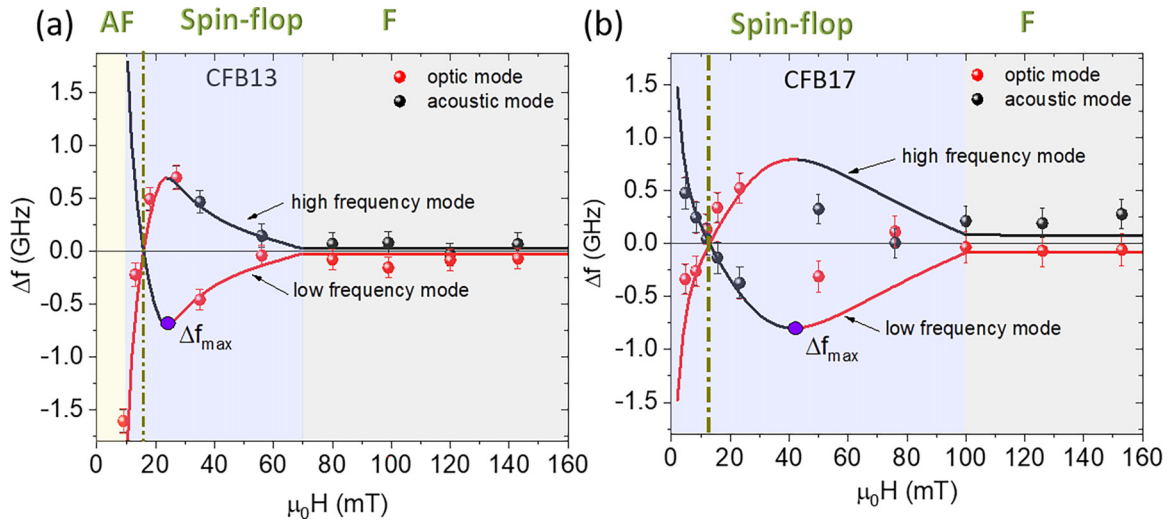


FIG. 4. Frequency nonreciprocity as a function of the magnetic field measured in CFB13 (a) and CFB17 (b) films. As in Fig. 3, differently colored areas indicate three magnetic states, within which frequency nonreciprocity shows different dependencies: it shows a maximum at AF state, peak formation in the spin-flop region, and zero nonreciprocity for ferromagnetic alignment. Vertical dashed lines indicate the magnetic field where Δf becomes zero.

In the case of the asymmetric CFB17 sample, the AF alignment cannot be fully achieved, and a moderate Δf is measured even at the smallest applied magnetic field. As in the previous sample, a nonmonotonous variation of Δf is found in the spin-flop regime, but, contrary to the symmetric sample, the frequency shift is not zero at large applied fields, indicating a breaking of symmetry along the thickness at such fields. We attribute such a finite Δf to a slight difference in the saturation magnetization of the layers, which implies that a small nonreciprocity remains for both layers being parallel.

Let us now concentrate on the nonmonotonous variation of the frequency nonreciprocity in the spin-flop region, which is the main finding of this study. In general, we may expect that the nonreciprocity Δf changes from a finite value to zero when transitioning from the AF state to the parallel state. However, this is not the case since a nontrivial nonmonotonous behavior is observed due to the dynamic dipolar interaction between the ferromagnetic layers. Indeed, in both samples, a sign reversal of the frequency shift is observed when the magnetization in both layers starts to rotate from AF to FM alignment, indicating the redistribution of the energy in the system. In other words, the spin waves propagating in a given direction with high energy (high group velocity) transform into waves with low energy when the relative magnetization switches from one canted state to another. While the sign reversal of the nonreciprocal frequency shift was previously demonstrated for different canted magnetization states obtained at different field polarities [29], in the present case the sign reversal occurs *at the same field polarity*, where different canted states are formed in the spin-flop regime.

The nonmonotonous dependence of the frequency nonreciprocity was also confirmed numerically, as shown by solid lines in Fig. 4. An excellent agreement was found for the CFB13 sample, and a reasonable agreement was reached for the CFB17 sample. The discrepancies observed between the model and the measurements for sample CFB17 [see Fig. 4(b)] can be attributed to a twisting of the magnetization

around the film's surface normal, which is feasible at a low external field (spin-flop region) in thicker samples. Upon increasing the thickness of the ferromagnet, as observed in exchange spring magnets [47,48], the magnetization is twisted, resulting in a noncollinear magnetic moment at the two interfaces of the ferromagnet. Nevertheless, the calculations for both samples, as the measurements, show that the frequency nonreciprocity exhibits a maximum Δf_{\max} at the precession phase interchange region. To gain more insight into the nonmonotonous nonreciprocity, the dynamic dipolar interaction of the low-frequency mode is calculated (see Appendix B for details). In Fig. 5(a), this dynamic interaction, $\varepsilon_d(k)$, is plotted for positive and negative k as a function of the magnetic field (see the dashed lines), while the solid line illustrates the dipolar interaction difference $\varepsilon_d(+k) - \varepsilon_d(-k)$. As the magnetic field increases, the angle between the magnetic moments of the FM layers changes, and the dipolar interaction increases for one direction of k and decreases for the opposite k . At the interception point, the difference in the dipolar energy for counterpropagating waves becomes zero, which explains a zero-frequency nonreciprocity at this field [see the vertical green line in Fig. 5(a)]. By further increasing the external magnetic field, the dipolar interaction steadily decreases for $k > 0$, while it approaches a maximum and then decreases for $k < 0$. Naturally, the difference in the dipolar energy for counterpropagating waves will exhibit a minimum and then gradually increase until reaching a constant value for parallel alignment of the magnetic moments. This dependence of the dynamic dipolar interaction on the magnetic field clearly reproduces the nonmonotonous dependence of Δf shown in Fig. 4. It is worth mentioning that in the case of the high-frequency mode, similar behavior is obtained, but in this case, $\varepsilon_d(+k) - \varepsilon_d(-k)$ exhibits a maximum close to $\mu_0 H = 23$ mT.

The dipolar origin of Δf suggests a strong dependence on the layer thicknesses. As one can see from Fig. 4, the maximum of the frequency nonreciprocity in the spin-flop regime

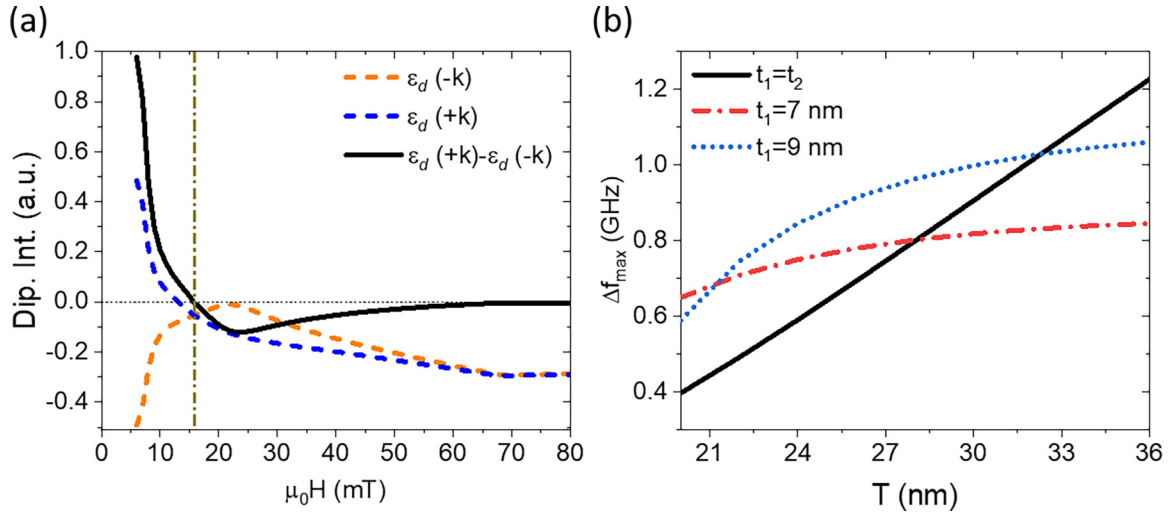


FIG. 5. (a) Dipolar interaction, $\varepsilon_d(k)$, as a function of magnetic field calculated for $k > 0$ (blue dashed line) and $k < 0$ (orange dashed line). The solid line depicts the dipolar interaction difference $\varepsilon_d(+k) - \varepsilon_d(-k)$ as a function of the magnetic field, while the vertical olive line illustrates the state where $\varepsilon_d(+k) - \varepsilon_d(-k) = 0$. The calculations are done using the magnetic parameters of sample CFB13. (b) Maximum of the frequency nonreciprocity Δf_{\max} vs total thickness of the two FM layers in the SAF $T = t_1 + t_2$. The solid line is for symmetric structure, $t_1 = t_2$, and the dashed and dotted lines are for asymmetric stack with fixed thickness for one layer.

Δf_{\max} is almost the same for both samples, demonstrating that the amplitude of Δf depends on the total thickness of the magnetic layers $T = t_1 + t_2$. Moreover, the dipolar nature implies that the amplitude of Δf scales linearly with the total thickness of the ferromagnetic layers, as shown in Fig. 5(b) by the solid line for the case of the symmetric SAF. Interestingly, by considering the asymmetric stack, the linear dependence transforms into a hyperbolic one, as can be seen from the calculations for the case of the fixed thickness of one of the layers and various thicknesses of the second layer.

IV. CONCLUSION

In this work, spin-wave dynamics were studied in symmetric as well as asymmetric in-plane CoFeB-based SAFs, where the relative orientation of magnetic moments in the two layers was tuned by an externally applied magnetic field along the in-plane easy axis. Using the Brillouin light-scattering technique, it was found that the frequency nonreciprocity, which occurs in the system due to the dipolar interaction between the layers, exhibits a nonmonotonous dependence in the spin-flop regime. This nontrivial dependence is explained by the nonmonotonous chiral dynamic dipolar interaction when the static magnetization transitions from the antiferromagnetic to the ferromagnetic state. Moreover, we have demonstrated that the frequency nonreciprocity can even change the sign without switching the polarity of the external magnetic field. These results extend the options within magnonic devices based on the nonreciprocal dynamic nature of spin waves by making use of the nonmonotonic field dependency effect.

ACKNOWLEDGMENTS

O.G. acknowledges the financial support from the DFG (SKYMAG project SCHU 2922/4-1). R.A.G. acknowledges the financial support from FONDECYT, Grant No. 1210607.

APPENDIX A: THEORY FOR THE SPIN-WAVE PROPAGATION IN SYNTHETIC ANTIFERROMAGNETS

The magnetization dynamic is obtained by using the Landau-Lifshitz (LL) equation of motion,

$$\dot{\mathbf{M}}^{(v)} = -\mu_0\gamma\mathbf{M}^{(v)} \times \mathbf{H}^{e(v)}, \quad (\text{A1})$$

where γ is the absolute value of the gyromagnetic ratio, $\mathbf{M}^{(v)}$ is the magnetization of layer v (being $v = 1, 2$), and $\mathbf{H}^{e(v)}$ is the effective field. Because the magnetizations of each layer can have different orientations, two coordinate systems are considered: (i) An orthogonal coordinate system (x, y, z) , where y is along the normal of the system, and x is along the in-plane easy axis. (ii) A local frame given by (X_v, Y_v, Z_v) wherein Z_v is along the equilibrium magnetization of layer v and $Y_v = y$. If there are small oscillations of magnetization around the equilibrium state, the magnetization vector and the effective field can be written as $\mathbf{M}^{(v)} = M_{sv}\hat{Z}_v + \mathbf{m}$ and $\mathbf{H}^{e(v)} = H_{Z_v}^{e0}\hat{Z}_v + \mathbf{h}^e$. Here, $\mathbf{m} = m_{X_v}\hat{X}_v + m_{Y_v}\hat{Y}_v$ is the dynamic magnetization, while \mathbf{h}^e is proportional to \mathbf{m} . Thus, assuming that $\mathbf{m} = \mathbf{m}(z)e^{i\omega t}$, with ω being the angular frequency, and neglecting second-order terms in $\mathbf{m}(z)$, the equations of motion by components read

$$i(\omega/\mu_0\gamma)m_{X_v}(z) = -m_{Y_v}(z)H_{Z_v}^{e0} + M_{sv}h_{Y_v}^e(z) \quad (\text{A2})$$

and

$$i(\omega/\mu_0\gamma)m_{Y_v}(z) = m_{X_v}(z)H_{Z_v}^{e0} - M_{sv}h_{X_v}^e(z). \quad (\text{A3})$$

Note that the z -dependence on the dynamic magnetization is related to the fact that the spin-wave propagation is

assumed to be along z so that $\mathbf{m}(z) = \mathbf{m}_k e^{ikz}$, with k being the wave vector. Also, equilibrium considerations establish that $H_{X_\nu}^{e0} = H_{Y_\nu}^{e0} = 0$. Equations (A2) and (A3) can be written as an eigenvalue problem, namely

$$\tilde{\mathbf{A}}\mathbf{m}_k = i(\omega/\mu_0\gamma)\mathbf{m}_k. \quad (\text{A4})$$

The matrix elements of $\tilde{\mathbf{A}}$ depend on the energetic interactions of the bilayer system. In the current case, such interactions are Zeeman, demagnetizing, perpendicular anisotropy, in-plane uniaxial anisotropy, and interlayer terms. The interlayer energies are associated with the bilinear interlayer exchange (with strength J_1), the biquadratic term (with strength J_2), and the dipolar interaction induced by both surface and volumetric dynamic magnetic charges in the opposite layer. The energy density of the bilinear and the biquadratic terms is given by

$$\varepsilon_J = -J_1 \frac{\mathbf{M}^{(1)}\mathbf{M}^{(2)}}{M_{s1}M_{s2}} - J_2 \left(\frac{\mathbf{M}^{(1)}\mathbf{M}^{(2)}}{M_{s1}M_{s2}} \right)^2, \quad (\text{A5})$$

where J_1 and J_2 are the bilinear and biquadratic coupling parameters, respectively. If J_1 dominates and if $J_1 < 0$, then $\mathbf{M}^{(1)}$ and $\mathbf{M}^{(2)}$ become antiparallel. On the other side, if J_2 dominates and is negative, then $\mathbf{M}^{(1)}$ and $\mathbf{M}^{(2)}$ tend to be perpendicular to each other.

Matrix elements can be found in the supplementary material in Ref. [27]. Here, the matrix elements are given by completeness:

$$\begin{aligned} A_{X_1}^{X_1} &= 0, \\ A_{Y_1}^{X_1} &= -M_{s1}\zeta(k, t_1) - M_{s1}[\lambda_{\text{ex}}^{(1)}]^2 k^2 - H_{Z_1}^{e0} - H_s^{(1)}, \\ A_{X_2}^{X_1} &= iM_{s1} \sin \varphi_2 \frac{kt_2}{2} \zeta(k, t_1)\zeta(k, t_2)e^{-|k|s}, \\ A_{Y_2}^{X_1} &= M_{s1} \frac{|k|t_2}{2} \zeta(k, t_1)\zeta(k, t_2)e^{-|k|s} + \frac{J_1 + 2J_2 \cos(\varphi_1 - \varphi_2)}{t_1\mu_0M_{s2}}. \end{aligned}$$

$$\begin{aligned} A_{X_1}^{Y_1} &= M_{s1} \sin^2 \varphi_1 [1 - \zeta(k, t_1)] + M_{s1}[\lambda_{\text{ex}}^{(1)}]^2 k^2 \\ &\quad - H_{u1} \cos^2 \varphi_1 + H_{Z_1}^{e0} - \frac{2J_2}{t_1\mu_0M_{s1}} \sin^2(\varphi_1 - \varphi_2), \end{aligned}$$

$$A_{Y_1}^{Y_1} = 0,$$

$$\begin{aligned} A_{X_2}^{Y_1} &= M_{s1} \sin \varphi_1 \sin \varphi_2 \frac{|k|t_2}{2} \zeta(k, t_1)\zeta(k, t_2)e^{-|k|s} \\ &\quad - \frac{J_1 \cos(\varphi_2 - \varphi_1) + 2J_2 \cos[2(\varphi_1 - \varphi_2)]}{t_1\mu_0M_{s2}}, \end{aligned}$$

$$A_{Y_2}^{Y_1} = -iM_{s1} \sin \varphi_1 \frac{kt_2}{2} \zeta(k, t_1)\zeta(k, t_2)e^{-|k|s};$$

$$A_{X_1}^{X_2} = -iM_{s2} \sin \varphi_1 \frac{kt_1}{2} \zeta(k, t_1)\zeta(k, t_2)e^{-|k|s},$$

$$A_{Y_1}^{X_2} = M_{s2} \frac{|k|t_1}{2} \zeta(k, t_1)\zeta(k, t_2)e^{-|k|s} + \frac{J_1 + 2J_2 \cos(\varphi_1 - \varphi_2)}{t_2\mu_0M_{s1}},$$

$$A_{X_2}^{X_2} = 0,$$

$$A_{Y_2}^{X_2} = -M_{s2}\zeta(k, t_2) - M_{s2}[\lambda_{\text{ex}}^{(2)}]^2 k^2 - H_{Z_2}^{e0} + H_s^{(2)};$$

$$\begin{aligned} A_{X_1}^{Y_2} &= M_{s2} \sin \varphi_1 \sin \varphi_2 \frac{|k|t_1}{2} \zeta(k, t_1)\zeta(k, t_2)e^{-|k|s} \\ &\quad - \frac{J_1 \cos(\varphi_1 - \varphi_2) + 2J_2 \cos[2(\varphi_1 - \varphi_2)]}{t_2\mu_0M_{s1}}, \end{aligned}$$

$$A_{Y_1}^{Y_2} = iM_{s2} \sin \varphi_2 \frac{kt_1}{2} \zeta(k, t_1)\zeta(k, t_2)e^{-|k|s},$$

$$\begin{aligned} A_{X_2}^{Y_2} &= M_{s2} \sin^2 \varphi_2 [1 - \zeta(k, t_2)] + M_{s2}[\lambda_{\text{ex}}^{(2)}]^2 k^2 - H_{u2} \cos^2 \varphi_2 \\ &\quad + H_{Z_2}^{e0} - \frac{2J_2}{t_2\mu_0M_{s2}} \sin^2(\varphi_1 - \varphi_2), \end{aligned}$$

$$A_{Y_2}^{Y_2} = 0$$

with

$$\zeta(k, t_\nu) = \frac{\sinh(|k|t_\nu/2)e^{-|k|t_\nu/2}}{|k|t_\nu/2} \quad (\text{A6})$$

and

$$\begin{aligned} H_{Z_\nu}^{e0} &= H \cos(\varphi_H - \varphi_\nu) + H_u^{(\nu)} \sin^2 \varphi_\nu \\ &\quad + \frac{J_1 \cos(\varphi_1 - \varphi_2) + 2J_2 \cos^2(\varphi_1 - \varphi_2)}{t_\nu\mu_0M_s^{(\nu)}}. \end{aligned}$$

t_ν is the thickness of layer ν and angle φ_ν corresponds to the angle between the z -axis (wave propagation) and the equilibrium magnetization of layer ν . One can note that when the equilibrium magnetizations are antiparallel, the angles are given by $\varphi_1 = \varphi_2 + \pi$, while in the parallel case $\varphi_1 = \varphi_2$. Nevertheless, in the spin-flop region, the angles are different ($\varphi_1 \neq \varphi_2$) so that they have to be found by utilizing the equilibrium conditions, which establish that the in-plane static effective field must be null ($H_{X_\nu}^{e0} = 0$). For the current system, it can be shown that

$$\begin{aligned} H_{X_\nu}^{e0} &= \frac{J_2 \sin[2(\varphi_\nu - \varphi_\eta)]}{t_\nu\mu_0M_{s\nu}} + \frac{J_1 \sin(\varphi_\nu - \varphi_\eta)}{t_\nu\mu_0M_{s\nu}} \\ &\quad - H \sin(\varphi_H - \varphi_\nu) - H_{u\nu} \sin(\varphi_\nu) \cos(\varphi_\nu), \end{aligned} \quad (\text{A7})$$

where if $\nu = 1$ ($\nu = 2$), then $\eta = 2$ ($\eta = 1$). Thus, once the equilibrium angle φ_ν is obtained from Eq. (A7), it is included in the matrix elements $A_{\xi_\nu}^{\xi'_\nu}$ to finally obtain the dynamics of the system.

APPENDIX B: NONRECIPROCAL DYNAMIC DIPOLAR INTERACTION

The interlayer dynamic dipolar interaction is a complex term, but its nature can be separated into two quantities: those that depend on the wave-vector sign (nonreciprocal terms) and those that do not. The nonreciprocal terms induce the nonreciprocity in the spin-wave dispersion; therefore, one can focus on such nonreciprocal dynamic dipolar interaction to analyze the frequency nonreciprocity. By analyzing Eqs. (A2) and (A3) together with matrix elements ($A_{\xi_\nu}^{\xi'_\nu}$), it can be shown that the effective dynamic fields associated with the

dipole-dipole energies are

$$h_{Y_\nu}^d = (-1)^\eta im_{X_\eta} \sin \varphi_\eta \frac{kt_\eta}{2} \zeta(k, t_\nu) \zeta(k, t_\eta) e^{-|k|s} \quad (\text{B1})$$

and

$$h_{X_\nu}^d = (-1)^\eta im_{Y_\eta} \sin \varphi_\nu \frac{kt_\eta}{2} \zeta(k, t_\nu) \zeta(k, t_\eta) e^{-|k|s}, \quad (\text{B2})$$

where if $\nu = 1$ ($\nu = 2$), then $\eta = 2$ ($\eta = 1$). One can see that under a change of sign in the wave vector, the dipolar fields also change their sign since they are proportional to the wave

vector k , while function $\zeta(k, t_\nu)$ depends on the wave-vector magnitude [see Eq. (A6)]. With the dipolar fields in hand, the dipolar interaction is given by

$$\varepsilon_d \propto \sum_{\nu \xi} m_{\xi_\eta}^* h_{\xi_\nu}^d, \quad (\text{B3})$$

where $\xi = X, Y$ and $\nu = 1, 2$. Note that the energy in Eq. (B3) is proportional to $m_{\xi_\eta}^* h_{\xi_\nu}^d$ because an explicit expression does not make sense here since, once that the matrix $\tilde{\mathbf{A}}$ is diagonalized, the magnetization components m_{ξ_η} are calculated in arbitrary units.

-
- [1] M. Jamali, J. H. Kwon, S.-M. Seo, K.-J. Lee, and H. Yang, Spin wave nonreciprocity for logic device applications, *Sci. Rep.* **3**, 3160 (2013).
- [2] F. Garcia-Sanchez, P. Borys, A. Vansteenkiste, J.-V. Kim, and R. L. Stamps, Nonreciprocal spin-wave channeling along textures driven by the Dzyaloshinskii-Moriya interaction, *Phys. Rev. B* **89**, 224408 (2014).
- [3] T. Brächer, O. Boulle, G. Gaudin, and P. Pirro, Creation of unidirectional spin-wave emitters by utilizing interfacial Dzyaloshinskii-Moriya interaction, *Phys. Rev. B* **95**, 064429 (2017).
- [4] F. Garcia-Sanchez, P. Borys, R. Soucaille, J.-P. Adam, R. L. Stamps, and J.-V. Kim, Narrow Magnonic Waveguides Based on Domain Walls, *Phys. Rev. Lett.* **114**, 247206 (2015).
- [5] J.-V. Kim, R. L. Stamps, and R. E. Camley, Spin Wave Power Flow and Caustics in Ultrathin Ferromagnets with the Dzyaloshinskii-Moriya Interaction, *Phys. Rev. Lett.* **117**, 197204 (2016).
- [6] R. Verba, V. Tiberkevich, and A. Slavin, Wide-Band Nonreciprocity of Surface Acoustic Waves Induced by Magnetoelastic Coupling with a Synthetic Antiferromagnet, *Phys. Rev. Appl.* **12**, 054061 (2019).
- [7] P. J. Shah, D. A. Bas, I. Lisenkov, A. Matyushov, N. X. Sun, and M. R. Page, Giant nonreciprocity of surface acoustic waves enabled by the magnetoelastic interaction, *Sci. Adv.* **6**, eabc5648 (2020).
- [8] A. Hernández-Mínguez, F. Macià, J. M. Hernández, J. Herfort, and P. V. Santos, Large Nonreciprocal Propagation of Surface Acoustic Waves in Epitaxial Ferromagnetic/Semiconductor Hybrid Structures, *Phys. Rev. Appl.* **13**, 044018 (2020).
- [9] M. Küß, M. Heigl, L. Flacke, A. Hörner, M. Weiler, A. Wixforth, and M. Albrecht, Nonreciprocal Magnetoacoustic Waves in Dipolar-Coupled Ferromagnetic Bilayers, *Phys. Rev. Appl.* **15**, 034060 (2021).
- [10] P. Che, I. Stasinopoulos, A. Mucchietto, J. Li, H. Berger, A. Bauer, C. Pfeleiderer, and D. Grundler, Confined dipole and exchange spin waves in a bulk chiral magnet with Dzyaloshinskii-Moriya interaction, *Phys. Rev. Res.* **3**, 033104 (2021).
- [11] S. Seki, Y. Okamura, K. Kondou, K. Shibata, M. Kubota, R. Takagi, F. Kagawa, M. Kawasaki, G. Tatara, Y. Otani, and Y. Tokura, Magnetochiral nonreciprocity of volume spin wave propagation in chiral-lattice ferromagnets, *Phys. Rev. B* **93**, 235131 (2016).
- [12] J.-H. Moon, S.-M. Seo, K.-J. Lee, K.-W. Kim, J. Ryu, H.-W. Lee, R. D. McMichael, and M. D. Stiles, Spin-wave propagation in the presence of interfacial Dzyaloshinskii-Moriya interaction, *Phys. Rev. B* **88**, 184404 (2013).
- [13] M. Belmuguenai, J.-P. Adam, Y. Roussigné, S. Eimer, T. Devolder, J.-V. Kim, S. M. Cherif, A. Stashkevich, and A. Thiaville, Interfacial Dzyaloshinskii-Moriya interaction in perpendicularly magnetized Pt/Co/AlOx ultrathin films measured by Brillouin light spectroscopy, *Phys. Rev. B* **91**, 180405(R) (2015).
- [14] A. K. Chaurasiya, C. Banerjee, S. Pan, S. Sahoo, S. Choudhury, J. Sinha, and A. Barman, Direct observation of interfacial dzyaloshinskii-moriya interaction from asymmetric spin-wave propagation in W/CoFeB/SiO2 heterostructures down to subnanometer CoFeB thickness, *Sci. Rep.* **6**, 32592 (2016).
- [15] R. A. Gallardo, P. Alvarado-Seguel, T. Schneider, C. Gonzalez-Fuentes, A. Roldán-Molina, K. Lenz, J. Lindner, and P. Landeros, Spin-wave non-reciprocity in magnetization-graded ferromagnetic films, *New J. Phys.* **21**, 033026 (2019).
- [16] J. A. Otálora, M. Yan, H. Schultheiss, R. Hertel, and A. Kákay, Curvature-Induced Asymmetric Spin-Wave Dispersion, *Phys. Rev. Lett.* **117**, 227203 (2016).
- [17] J. A. Otálora, M. Yan, H. Schultheiss, R. Hertel, and A. Kákay, Asymmetric spin-wave dispersion in ferromagnetic nanotubes induced by surface curvature, *Phys. Rev. B* **95**, 184415 (2017).
- [18] D. D. Sheka, O. V. Pylypovskiy, P. Landeros, Y. Gaididei, A. Kákay, and D. Makarov, Nonlocal chiral symmetry breaking in curvilinear magnetic shells, *Commun. Phys.* **3**, 128 (2020).
- [19] L. Körber, G. Quasebarth, A. Otto, and A. Kákay, Finite-element dynamic-matrix approach for spin-wave dispersions in magnonic waveguides with arbitrary cross section, *AIP Adv.* **11**, 095006 (2021).
- [20] L. Körber and A. Kákay, Numerical reverse engineering of general spin-wave dispersions: Bridge between numerics and analytics using a dynamic-matrix approach, *Phys. Rev. B* **104**, 174414 (2021).
- [21] R. A. Gallardo, P. Alvarado-Seguel, and P. Landeros, High spin-wave asymmetry and emergence of radial standing modes in thick ferromagnetic nanotubes, *Phys. Rev. B* **105**, 104435 (2022).
- [22] R. Verba, V. Tiberkevich, E. Bankowski, T. Meitzler, G. Melkov, and A. Slavin, Conditions for the spin wave nonreciprocity in an array of dipolarly coupled magnetic nanopillars, *Appl. Phys. Lett.* **103**, 082407 (2013).

- [23] K. Mika and P. Grünberg, Dipolar spin-wave modes of a ferromagnetic multilayer with alternating directions of magnetization, *Phys. Rev. B* **31**, 4465 (1985).
- [24] P. Grünberg, R. Schreiber, Y. Pang, M. B. Brodsky, and H. Sowers, Layered Magnetic Structures: Evidence for Antiferromagnetic Coupling of Fe Layers across Cr Interlayers, *Phys. Rev. Lett.* **57**, 2442 (1986).
- [25] P. X. Zhang and W. Zinn, Spin-wave modes in antiparallel magnetized ferromagnetic double layers, *Phys. Rev. B* **35**, 5219 (1987).
- [26] G. Binasch, P. Grünberg, F. Saurenbach, and W. Zinn, Enhanced magnetoresistance in layered magnetic structures with antiferromagnetic interlayer exchange, *Phys. Rev. B* **39**, 4828 (1989).
- [27] R. A. Gallardo, T. Schneider, A. K. Chaurasiya, A. Oelschlägel, S. S. P. K. Arekapudi, A. Roldán-Molina, R. Hübner, K. Lenz, A. Barman, J. Fassbender, J. Lindner, O. Hellwig, and P. Landeros, Reconfigurable Spin-Wave Nonreciprocity Induced by Dipolar Interaction in a Coupled Ferromagnetic Bilayer, *Phys. Rev. Appl.* **12**, 034012 (2019).
- [28] V. Sluka, T. Schneider, R. A. Gallardo, A. Kákay, M. Weigand, T. Warnatz, R. Mattheis, A. Roldán-Molina, P. Landeros, V. Tiberkevich, A. Slavin, G. Schütz, A. Erbe, A. Deac, J. Lindner, J. Raabe, J. Fassbender, and S. Wintz, Emission and propagation of 1d and 2d spin waves with nanoscale wavelengths in anisotropic spin textures, *Nat. Nanotechnol.* **14**, 328 (2019).
- [29] M. Ishibashi, Y. Shiota, T. Li, S. Funada, T. Moriyama, and T. Ono, Switchable giant nonreciprocal frequency shift of propagating spin waves in synthetic antiferromagnets, *Sci. Adv.* **6**, eaaz6931 (2020).
- [30] E. Albisetti, S. Tacchi, R. Silvani, G. Scaramuzzi, S. Finizio, S. Wintz, C. Rinaldi, M. Cantoni, J. Raabe, G. Carlotti, R. Bertacco, E. Riedo, and D. Petti, Optically inspired nanomagnonics with nonreciprocal spin waves in synthetic antiferromagnets, *Adv. Mater.* **32**, 1906439 (2020).
- [31] R. A. Gallardo, P. Alvarado-Seguel, A. Kákay, J. Lindner, and P. Landeros, Spin-wave focusing induced by dipole-dipole interaction in synthetic antiferromagnets, *Phys. Rev. B* **104**, 174417 (2021).
- [32] M. Grassi, M. Geilen, D. Louis, M. Mohseni, T. Brächer, M. Hehn, D. Stoeffler, M. Bailleul, P. Pirro, and Y. Henry, Slow-Wave-Based Nanomagnonic Diode, *Phys. Rev. Appl.* **14**, 024047 (2020).
- [33] R. Zivieri, L. Giovannini, and P. Vavassori, Theory of Brillouin cross section from magnetic nanostructured multilayers, in *Magnetic Nanostructures*, edited by H. S. Nalwa (American Scientific, California, 2002), Chap. 3.
- [34] K. Di, S. X. Feng, S. N. Piramanayagam, V. L. Zhang, H. S. Lim, S. C. Ng, and M. H. Kuok, Enhancement of spin-wave nonreciprocity in magnonic crystals via synthetic antiferromagnetic coupling, *Sci. Rep.* **5**, 10153 (2015).
- [35] P. Alvarado-Seguel and R. A. Gallardo, Band structure of a one-dimensional bilayer magnonic crystal, *Phys. Rev. B* **100**, 144415 (2019).
- [36] P. Gruszecki, C. Banerjee, M. Mruczkiewicz, O. Hellwig, A. Barman, and M. Krawczyk, The influence of the internal domain wall structure on spin wave band structure in periodic magnetic stripe domain patterns, *Solid State Phys.* **70**, 79 (2019).
- [37] Y. Henry, D. Stoeffler, J.-V. Kim, and M. Bailleul, Unidirectional spin-wave channeling along magnetic domain walls of Bloch type, *Phys. Rev. B* **100**, 024416 (2019).
- [38] J. C. Slonczewski, Current-driven excitation of magnetic multilayers, *J. Magn. Magn. Mater.* **159**, L1 (1996).
- [39] M. Belmeguenai, T. Martin, G. Woltersdorf, M. Maier, and G. Bayreuther, Frequency- and time-domain investigation of the dynamic properties of interlayer-exchange-coupled Ni₈₁Fe₁₉/Ru/Ni₈₁Fe₁₉ thin films, *Phys. Rev. B* **76**, 104414 (2007).
- [40] S. J. Yun, S. H. Lim, and S.-R. Lee, Strong interlayer exchange coupling and high post-annealing stability in perpendicularly magnetized [Pt/Co]/Ru/[Co/Pt] structures, *AIP Adv.* **6**, 025112 (2016).
- [41] B. K. Kuanr, M. Buchmeier, R. R. Gareev, D. E. Bürgler, R. Schreiber, and P. Grünberg, Spin-wave modes and line broadening in strongly coupled epitaxial Fe/Al/Fe and Fe/Si/Fe trilayers observed by Brillouin light scattering, *J. Appl. Phys.* **93**, 3427 (2003).
- [42] Z. Zhang, L. Zhou, P. E. Wigen, and K. Ounadjela, Angular dependence of ferromagnetic resonance in exchange-coupled Co/Ru/Co trilayer structures, *Phys. Rev. B* **50**, 6094 (1994).
- [43] S. van Dijken, G. D. Santo, and B. Poelsema, Influence of the deposition angle on the magnetic anisotropy in thin Co films on Cu(001), *Phys. Rev. B* **63**, 104431 (2001).
- [44] S. Li, Q. Xue, J.-G. Duh, H. Du, J. Xu, Y. Wan, Q. Li, and Y. Lü, Driving ferromagnetic resonance frequency of FeCoB/PZn-PT multiferroic heterostructures to Ku-band via two-step climbing: composition gradient sputtering and magnetoelectric coupling, *Sci. Rep.* **4**, 7393 (2014).
- [45] S. Sorokin, R. A. Gallardo, C. Fowley, K. Lenz, A. Titova, G. Y. P. Atcheson, G. Dennehy, K. Rode, J. Fassbender, J. Lindner, and A. M. Deac, Magnetization dynamics in synthetic antiferromagnets: Role of dynamical energy and mutual spin pumping, *Phys. Rev. B* **101**, 144410 (2020).
- [46] M. Belmeguenai, T. Martin, G. Woltersdorf, G. Bayreuther, V. Baltz, A. K. Suszka, and B. J. Hickey, Microwave spectroscopy with vector network analyzer for interlayer exchange-coupled symmetrical and asymmetrical NiFe/Ru/NiFe, *J. Phys.: Condens. Matter* **20**, 345206 (2008).
- [47] O. Hellwig, J. B. Kortright, K. Takano, and E. E. Fullerton, Switching behavior of Fe-Pt/Ni-Fe exchange-spring films studied by resonant soft-x-ray magneto-optical Kerr effect, *Phys. Rev. B* **62**, 11694 (2000).
- [48] E. E. Fullerton, J. S. Jiang, and S. D. Bader, Hard/soft magnetic heterostructures: Model exchange-spring magnets, *J. Magn. Magn. Mater.* **200**, 392 (1999).